Progress In Electromagnetics Research M, Vol. 96, 1–8, 2020

Boundary Value-Free Magnetic Resonance Electrical Properties Tomography Based on the Generalized Cauchy Formula with the Complex-derivative Boundary Condition

Motofumi Fushimi* **and Takaaki Nara**

Abstract—Recently, magnetic-resonance-based electrical properties tomography, by which the electrical properties (EPs), namely conductivity and permittivity, of biological tissues are reconstructed, has been an active area of study. We previously proposed an explicit reconstruction method based on the Dbar equation and its explicit solution given by the generalized Cauchy formula. In this method, as in some other conventional methods, the values of EPs on the boundary of the region of interest must be specified by the Dirichlet boundary condition of the partial differential equation. However, it is difficult to know the precise values in practical situations. In this paper, we propose a novel method that reconstructs EPs without the prior information of boundary EP values by deriving a new representation formula of the solution of the Dbar equation with the complex-derivative boundary condition. Numerical simulations and phantom experiments show that the proposed method can reconstruct EPs without knowledge of the boundary EP values. Therefore, the proposed method greatly enhances the applicability of the current EPT methods to practical situations.

1. INTRODUCTION

Electrical properties (EPs), namely electric conductivity and dielectric permittivity, of biological tissues provide valuable information for clinical diagnoses of cancerous tissues [1–3]. Among several techniques to noninvasively image EPs, electrical impedance tomography (EIT) has been well studied in the past decades. The main limitation of EIT is that the resolution of the reconstructed image is low due to the ill-posed nature of the inversion from the surface measurement [4].

Recently, electrical properties tomography (EPT) based on magnetic resonance imaging (MRI) has attracted attention as an emerging modality that noninvasively reconstructs the electrical properties of biological tissues from the magnetic field inside the body measured using an MRI scanner [5, 6]. The electromagnetic fields transmitted by radiofrequency coils are governed by the following time-harmonic Maxwell's equations:

$$\nabla \times \mathbf{E}(\mathbf{r}) = -\mathrm{i}\omega\mu_0\mathbf{H}(\mathbf{r}), \tag{1}$$

$$\nabla \times \mathbf{H}(\mathbf{r}) = \mathrm{i}\omega\left(\epsilon_r(\mathbf{r})\epsilon_0 - \mathrm{i}\frac{\sigma(\mathbf{r})}{\omega}\right)\mathbf{E}(\mathbf{r}) = \mathrm{i}\omega\kappa(\mathbf{r})\mathbf{E}(\mathbf{r}), \tag{2}$$

where $\mathbf{r} \in \Omega$ and Ω represents the body. μ_0 and ϵ_0 are the magnetic permeability and dielectric permittivity of free space, respectively, and $\omega/2\pi$ is the Larmor frequency of proton nuclei. We define the complex permittivity, κ, as $\epsilon_r\epsilon_0 - \mathrm{i}\sigma/\omega$, where ϵ_r and σ are relative permittivity and conductivity, respectively. The magnetic permeability is assumed to be constant and identical to μ_0 throughout the entire body [7]. Using receiver coils, the positively rotating component of the magnetic field,

Received 22 June 2020, Accepted 9 August 2020, Scheduled 22 August 2020
* Corresponding author: Motofumi Fushimi (motofumi-fushimi@g.ecc.u-tokyo.ac.jp).
The authors are with the Graduate School of Information Science and Technology, The University of Tokyo, Japan.

$H^+ \equiv (H_x + \mathrm{i}H_y)/2$, where the z-axis is set parallel to the body axis, can be measured inside Ω. Therefore, the EPT problem is to reconstruct κ inside the region of interest (ROI) denoted by $D \subset \Omega$ from the measured H^+ data.

A typical approach for the EPT problem is to derive Helmholtz's equation for H^+ by neglecting the spatial variation of κ [8, 9]. However, it has been reported that serious artifacts appear at tissue transition regions where EPs vary [10].

Several methods for removing the artifacts have been proposed [11–14]. Balidemaj et al. proposed the contrast source inversion EPT (CSI-EPT) method [12], in which the nonlinear integral equations for EPs and the electric field are solved in an iterative manner. As pointed by Arduino et al. [13], a linear partial differential equation (PDE) must be solved at each iteration by the finite element method (FEM) to properly account for the radiofrequency shield of the MRI coil, making its computational cost very high. Hampe et al. proposed the dictionary based EPT (bd-EPT) method, in which EPs are reconstructed so that the measured magnetic field pattern matches with the dictionary data constructed by simulations in advance [14]. Although bd-EPT showed superior noise behavior, the effectiveness of the method for the cases not included in the dictionary data is still unclear. Hafalir et al. proposed the cr-MREPT method [11], in which a linear PDE for the inverse of κ is solved by the FEM. This method can reconstruct EPs directly without iterative calculations nor the dictionary data. However, EP values on the boundary of the ROI must be given as the Dirichlet boundary condition (BC) of the PDE. Moreover, the Laplacian of the measured magnetic field data must be calculated, which amplifies noise.

We previously proposed a Dbar-equation-based reconstruction method [15, 16]. In this method, with the two-dimensional (2D) plane approximation $H_z = 0$ and $\partial_z H^+ = 0$, the following complex form of Maxwell's equations was derived:

$$\bar{\partial} E_z(\zeta) = \omega\mu_0 H^+(\zeta), \tag{3}$$

$$4\partial H^+(\zeta) = -\omega\kappa(\zeta) E_z(\zeta), \tag{4}$$

where $\zeta = x + \mathrm{i}y$, $\zeta \in D$ (D begins 2D ROI), and ∂ and $\bar{\partial}$ are the complex differential operators defined by

$$\partial \equiv \frac{1}{2}(\partial_x - \mathrm{i}\partial_y), \quad \bar{\partial} \equiv \frac{1}{2}(\partial_x + \mathrm{i}\partial_y). \tag{5}$$

In this method, first, we solve Eq. (3) for E_z. This type of PDE is known as the Dbar equation. An explicit representation of the solution is given by the generalized Cauchy formula [17]. Once we obtain E_z, κ is directly reconstructed as the ratio of ∂H^+ to E_z from Ampere's law as given in Eq. (4). Because this method does not need to calculate the second derivative of H^+, it is more robust against noise.

However, in this method, as in the cr-MREPT method, EP values on the boundary of the ROI must be specified, limiting the applicability of the method in practical situations. In this paper, we propose a reconstruction method that does not require boundary EP values. To this end, we solve the Dbar equation with the boundary value of the complex-derivative of the electric field instead of giving the Dirichlet boundary values of EPs. This is a generalization of our previous method [16] that solves the Neumann problem without the Dirichlet boundary value, although that method is valid only for the special case that the ROI is a circular domain.

2. THEORY

2.1. An Explicit Solution of the Dbar Equation with a Complex-Derivative Boundary Condition

In this section, we derive the representation formula of the solution of the Dbar equation with a complex-derivative BC.

Let D be a domain whose boundary and C a smooth Jordan curve. If ϕ is a holomorphic function in D and continuous in $\overline{D}$, then $\partial\phi$ is also holomorphic, and thus, the following Cauchy formula holds:

$$\partial\phi(\zeta) = \frac{1}{2\pi\mathrm{i}} \int_C \frac{\partial\phi(\zeta')}{\zeta' - \zeta} \mathrm{d}\zeta', \tag{6}$$

where $\zeta' = x' + \mathrm{i}y'$. By integrating both sides of Eq. (6) with respect to ζ, it follows that

$$\phi(\zeta) = -\frac{1}{2\pi\mathrm{i}} \int_C \log\left(1 - \frac{\zeta}{\zeta'}\right) \partial\phi(\zeta')\mathrm{d}\zeta' + c, \tag{7}$$

where c is a complex constant. This is a representation formula of a holomorphic function ϕ in D by $\partial\phi$ on C. In contrast to the ordinary Cauchy formula, which represents ϕ by the value of ϕ itself on the boundary, Eq. (6) uses the boundary value of its complex derivative $\partial\phi$.

Next, we extend Eq. (6) to the case of a function f that is not necessarily holomorphic in D. Following Vekua [17], we introduce the following integral operators:

$$T[f](\zeta) \equiv -\frac{1}{\pi} \iint_D \frac{f(\zeta')}{\zeta' - \zeta}\,\mathrm{d}x'\mathrm{d}y', \tag{8}$$

$$\Pi[f](\zeta) \equiv -\frac{1}{\pi} \iint_D \frac{f(\zeta')}{(\zeta' - \zeta)^2}\,\mathrm{d}x'\mathrm{d}y', \tag{9}$$

where the integrals have been proved to exist in the sense of Cauchy's principal value integral [17]. Here, the derivatives of $T[f]$ are represented as follows [17]:

$$\bar{\partial}T[f] = f, \tag{10}$$

$$\partial T[f] = \Pi[f]. \tag{11}$$

Then, it is easy to see that $f - T[\bar{\partial}f]$ is holomorphic since

$$\bar{\partial}(f - T[\bar{\partial}f]) = \bar{\partial}f - \bar{\partial}T[\bar{\partial}f] = \bar{\partial}f - \bar{\partial}f = 0. \tag{12}$$

Therefore, we can apply Eq. (7) to $f - T[\bar{\partial}f]$, giving our main result of this paper:

$$f(\zeta) = -\frac{1}{2\pi\mathrm{i}} \int_C \log\left(1 - \frac{\zeta}{\zeta'}\right) (\partial f(\zeta') - \Pi[\bar{\partial}f](\zeta'))\mathrm{d}\zeta' - \frac{1}{\pi} \iint_D \frac{\bar{\partial}f(\zeta')}{\zeta' - \zeta}\,\mathrm{d}x'\mathrm{d}y' + c. \tag{13}$$

This is a representation formula of a function f not necessarily holomorphic in terms of its complex derivative ∂f on the boundary and $\bar{\partial}f$ inside the region. In other words, in contrast to the generalized Cauchy formula, which solves the Dbar equation with the Dirichlet BC, Eq. (13) solves the Dbar equation with the complex-derivative BC. In our previous method [16], we used the Neumann derivative $\partial_n f$, where ∂_n represents the normal derivative on C. Thus, the previous representation formula was only valid for a circular region. Eq. (13) is, on the other hand, valid for regions of any shape.

2.2. Reconstruction Formula without the Boundary Value of EPs

In this section, we apply Eq. (13) to the EPT problem and derive the reconstruction formula of EPs that does not require boundary EP values.

By taking the $(x - \mathrm{i}y)$-component of Eq. (1), it holds that

$$\partial E_z = -\omega\mu_0 H^- + \partial_z E^- = -\omega\mu_0 H^- - \frac{\partial_z H^-}{4\bar{\partial}H^-}\,E_z, \tag{14}$$

where $E^- \equiv (E_x - \mathrm{i}E_y)/2$ and $H^- \equiv (H_x - \mathrm{i}H_y)/2$. Here, we use the relations $\partial_z H^- = -\omega\kappa E^-$ and $4\bar{\partial}H^- = \omega\kappa E_z$, which are deduced by taking the $(x - \mathrm{i}y)$- and z-components of Eq. (2). Thus, under the assumption that $\partial_z H^- = 0$, we get

$$\partial E_z = -\omega\mu_0 H^-. \tag{15}$$

Applying $f = E_z$ to Eq (13), we have

$$E_z(\zeta) = -\frac{1}{2\pi\mathrm{i}} \int_C \log\left(1 - \frac{\zeta}{\zeta'}\right) \left(\omega\mu_0 H^- - \Pi[\omega\mu_0 H^+](\zeta')\right) \mathrm{d}\zeta' - \frac{1}{\pi} \iint_D \frac{\omega\mu_0 H^+(\zeta')}{\zeta' - \zeta}\,\mathrm{d}x'\mathrm{d}y' + c, \tag{16}$$

since $\bar{\partial}E_z$ and ∂E_z are given by Eqs. (3) and (15), respectively. It is known that $|H^+| \gg |H^-|$ when the body is excited using a quadrature birdcage coil (QBC), which is commonly used in modern

MRI systems [18]. Hence, substituting Eqs. (3) and (15) into Eq. (13) under the condition that $|H^-| \ll |\Pi[H^+]|$ gives

$$E_z(\zeta) = \frac{1}{2\pi \mathrm{i}} \int_C \log\left(1 - \frac{\zeta}{\zeta'}\right) \Pi[\omega\mu_0 H^+](\zeta')\mathrm{d}\zeta' - \frac{1}{\pi}\iint_D \frac{\omega\mu_0 H^+(\zeta')}{\zeta' - \zeta}\,\mathrm{d}x'\mathrm{d}y' + c. \tag{17}$$

The validity of the assumption $|H^-| \ll |\Pi[H^+]|$ is shown using numerical simulations in Section 4. Eq. (17) gives E_z using only H^+ up to a constant c.

The constant c can be determined as follows. It is known that in the QBC setting, the zero point of E_z appears around the center of the body [11]. Accordingly, from Eq. (4), $\partial H^+ = 0$ here. From this fact, we determine the zero point ζ^* of E_z as the point where ∂H^+, which is computed from the measured H^+, is minimal as follows:

$$\zeta^* = \arg\min_{\zeta \in D} \left|\partial H^+(\zeta)\right|. \tag{18}$$

Then, c is obtained from

$$\begin{aligned} E_z(\zeta^*) \;=\; & -\frac{1}{2\pi \mathrm{i}} \int_C \log\left(1 - \frac{\zeta^*}{\zeta'}\right) (\omega\mu_0 H^-(\zeta') + \Pi[\omega\mu_0 H^+](\zeta'))\mathrm{d}\zeta' \\ & -\frac{1}{\pi}\iint_D \frac{\omega\mu_0 H^+(\zeta')}{\zeta' - \zeta^*}\,\mathrm{d}x'\mathrm{d}y' + c = 0. \end{aligned} \tag{19}$$

Using this c, E_z can be determined uniquely by Eq. (17). Once E_z is obtained, κ can be directly calculated as a ratio of $-4\partial H^+$ to ωE_z according to Eq. (4). Here, we estimate κ using the total variation regularization by minimizing the function

$$\hat{\kappa}(\zeta) = \arg\min_{\kappa} \left\|4\partial H^+(\zeta) + \omega E_z(\zeta)\right\|_2^2 + \lambda \left\||\nabla\kappa(\zeta)|\right\|_1 \tag{20}$$

to suppress the artifact caused by the zero point of E_z [11].

3. METHODS

3.1. Numerical Simulations

Following the method proposed by Gurler and Ider [19], a 16-leg high-pass shielded QBC was constructed, and two phantoms (a cylindrical phantom and the Shepp-Logan phantom [20]) were loaded into the coil. The magnetic field was excited at 123.2 MHz. H^+ was obtained on a 180 mm × 180 mm square region centered at the origin with a matrix size of 128×128 for both phantoms. Both phantoms have a few inclusions where EPs are different from those of the background region. Specifically, the cylindrical phantom has three cylindrical inclusions whose radii are 5 mm, 10 mm, and 15 mm, and heights are all 20 mm. The EP values are $(\sigma, \epsilon_r) = (1\,\mathrm{S/m}, 50)$ for the inclusions and $(\sigma, \epsilon_r) = (0.5\,\mathrm{S/m}, 80)$ for the background. We set the ROIs in a way that these inclusions were on the boundaries of the ROIs as shown in Figs. 2(a) and 3(a).

The computation of H^+ was performed using the FEM software, COMSOL Multiphysics 5.3 (COMSOL Inc.). MATLAB R2019a (The MathWorks Inc.) was used for all reconstruction processes.

3.2. Phantom Experiments

A phantom composed of two cylindrical regions (inner and outer regions) was used. The conductivity of the phantom was adjusted by adding NaCl. The conductivities of the inner and outer regions were 0.94 and 0.43 S/m, respectively, as measured using a conductivity meter (HI 8733, Hanna Instruments). The permittivity was constant and identical to that of water.

The magnitude of H^+ can be measured using the B1 mapping technique. We used the double angle method proposed in [21]. Note that we used the transceive phase approximation [18] to extract transmit phase $\angle H^+$ from the transceive phase. We set the ROI in a way that the inner region intersected the boundary in order to consider the practical situations where the positions of the inclusions are unknown.

The experiment was conducted using the 3 T MR scanner Magnetom Prisma (Siemens) at the University of Tokyo.

4. RESULTS

4.1. Simulation Results

Figure 1 shows the H^+ and H^- maps obtained from the FEM calculation. As shown in Figs. 1(c) and (d), $|H^-| \ll |H^+|$ and $|H^-| \ll |\Pi[H^+]|$ hold well. Note that the assumption that $|H^-| \ll |\Pi[H^+]|$ needs to hold only on the boundary of the ROI.

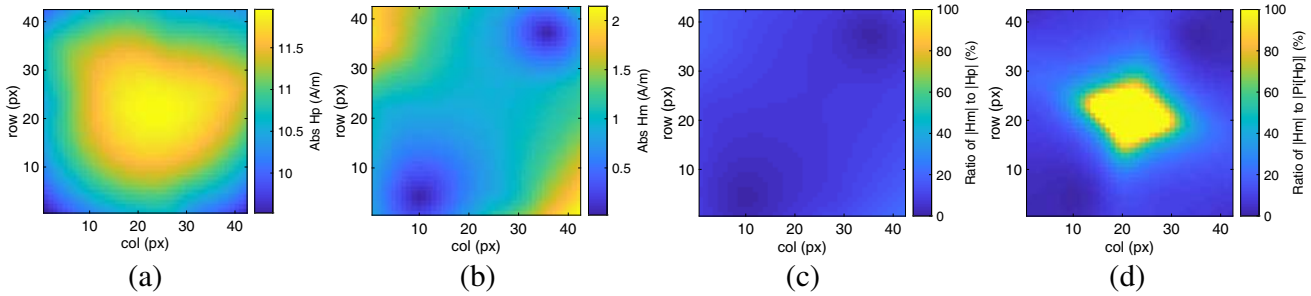

Figure 1. Magnitude of magnetic field maps and their ratio for the cylindrical phantom. (a) $|H^+|$, (b) $|H^-|$, (c) $|H^-|/|H^+|$, and (d) $|H^-|/|\Pi[H^+]|$.

Figure 2 shows the reconstruction results for the cylindrical phantom when 1% Gaussian noise was added. As shown in Fig. 2(b), the previous method with the true boundary EP values yields accurate results throughout the ROI. However, when the BC was specified as the background value of the true EPs on the boundary, which would be the most natural choice, the reconstructed images were distorted, as shown in Fig. 2(c). In contrast, the proposed method keeps the image quality as shown in Fig. 2(d).

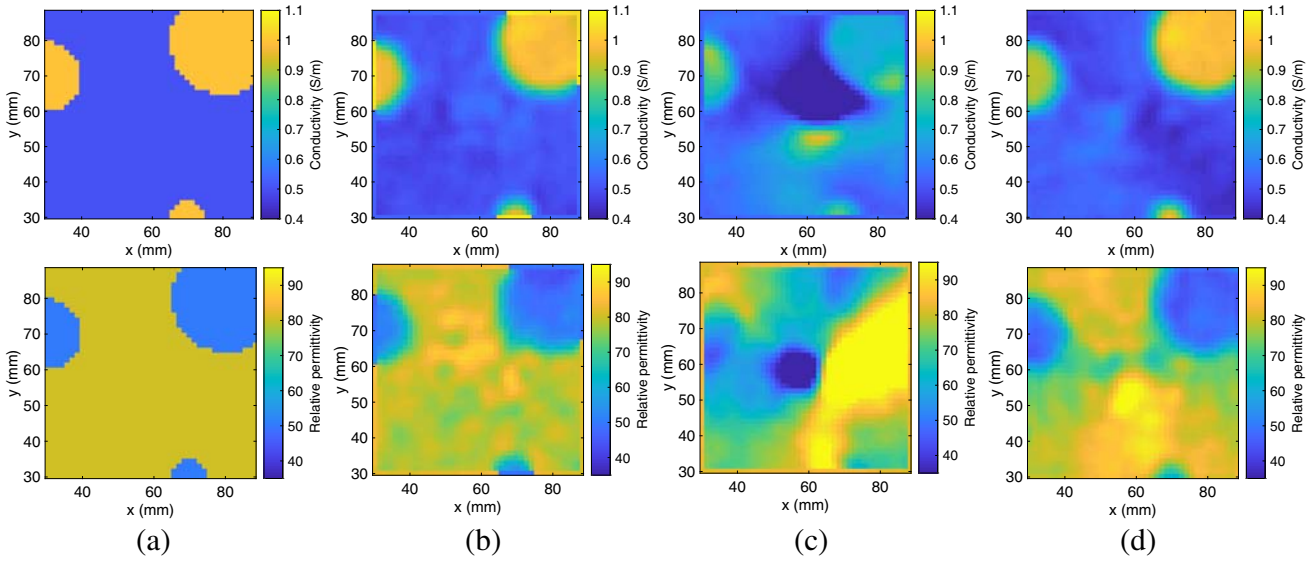

Figure 2. Reconstruction results of (top) conductivity and (bottom) relative permittivity for the cylindrical phantom and a signal-to-noise ratio of 40 dB. (a) True, (b) previous method with the true BC, (c) previous method with the background BC, and (d) proposed method.

Figure 3 shows the reconstruction results of the Shepp-Logan phantom. As in the case of the cylindrical phantom, the results of the proposed method are less distorted, and two small inclusions near the center are properly reconstructed, whereas large errors occur at these inclusions in the previous method with the average BC.

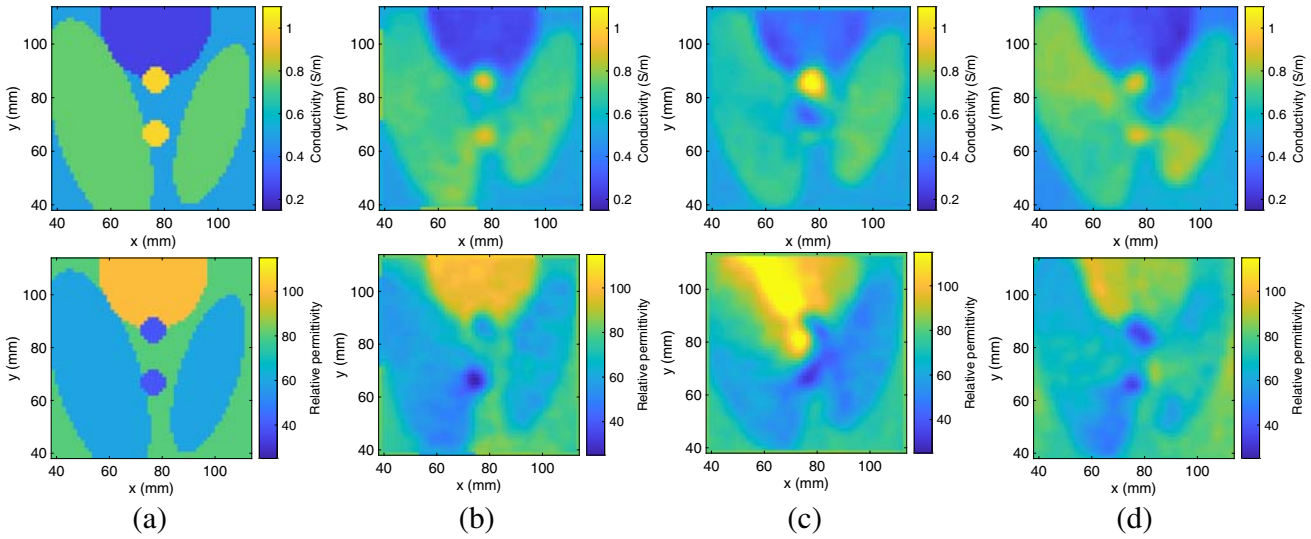

Figure 3. Reconstruction results of (top) conductivity and (bottom) relative permittivity for the Shepp-Logan phantom and a signal-to-noise ratio of 40 dB. (a) True, (b) previous method with the true BC, (c) previous method with the background BC, and (d) proposed method.

Table 1. Variance of relative error maps for the simulation phantoms. Units are $(\mathrm{S/m})^2$ for conductivity.

		True BC	Background BC	Proposed Method
Cylinder	Conductivity	0.0054	0.0316	0.0055
	Permittivity	0.0035	0.0888	0.0043
Shepp-Logan	Conductivity	0.0146	0.0491	0.0236
	Permittivity	0.0105	0.0298	0.0079

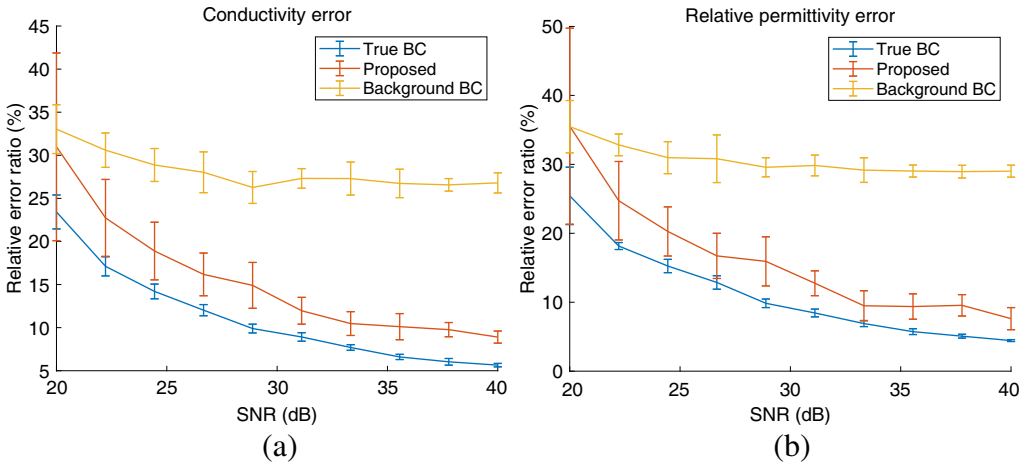

Figure 4. Reconstruction errors of (a) conductivity and (b) relative permittivity for the cylindrical phantom with a signal-to-noise ratio of 20–40 dB.

Table 1 shows the variances of the relative L^2 error of each result. We observe that the proposed method has smaller variance for both phantoms, which means that the proposed method yielded better results throughout the ROI. We also tested the proposed method on the cylindrical phantom with different SNR between 20 dB and 40 dB. Figure 4 shows the relative L^2 error of the conductivity and relative permittivity. The proposed method consistently has lower errors than the previous method with

the background BC. It should be emphasized that the reconstruction results of our proposed method are comparable to those of the previous method with the non-practical assumption that the true boundary values of EPs are available. In contrast to the previous method, the proposed method does not use any prior information of the boundary EP values, which means that the proposed method greatly enhances the applicability of EPT to practical situations.

4.2. Experimental Results

Figure 5 shows the reconstructed conductivities of the experimental phantom. As shown in Fig. 5(b), large error appears in the inner regions when the boundary EP values are given as the background value. The proposed method yields a less distorted map even when no information of the EP values on the boundary is given.

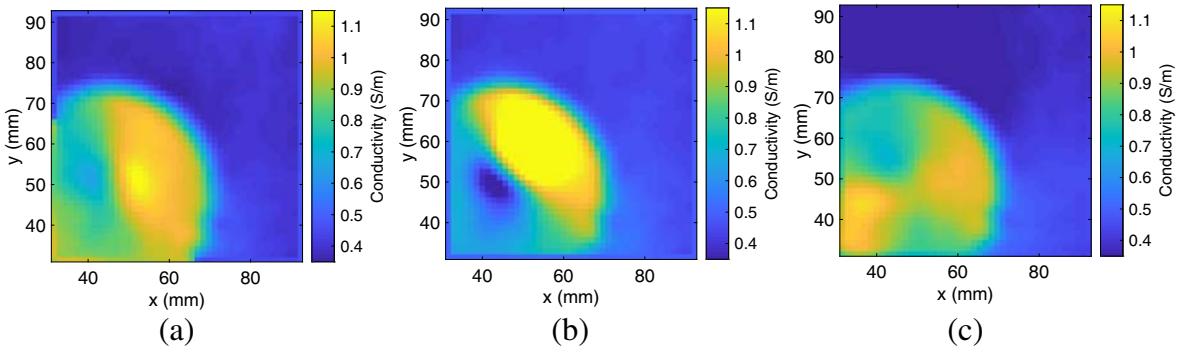

Figure 5. Reconstruction results of conductivity for the phantom experiment. (a) Previous method with the true BC, (b) previous method with the background BC, and (c) proposed method.

5. CONCLUSION

In this paper, we propose an explicit reconstruction method for EPT that does not require the prior information of EPs on the boundary of the ROI. The proposed method solves the Dbar equation with the novel complex-derivative BC instead of the Dirichlet BC. By assuming that $|H^-| \ll |\Pi[H^+]|$, EPs were reconstructed from only the measurable quantity, H^+ without the prior information of the EP values on the boundary of the ROI. This is the generalization of our previous method using the Neumann BC, which restricted to the special case of a circular-shaped ROI and can be applied to an arbitrarily-shaped ROI. Although EPT reconstruction without boundary EP values on a general-shaped ROI is fully accomplished by introducing the complex-derivative BC, other BCs such as Robin BC, which is the combination of Dirichlet and Neumann BCs, may be considered depending on applications. Numerical simulations and phantom experiments showed that the proposed method can reconstruct EPs without the prior information of EPs on the boundary on the ROI. Currently, the proposed method is restricted to two-dimensional problems where the object has homogeneous EPs along the body axis, and thus, future work is to extend the method to the general three-dimensional problems.

ACKNOWLEDGMENT

This work was partly supported by JSPS KAKENHI Grant Number 19H04438.

REFERENCES

1. Joines, W. T., Y. Zhang, C. Li, and R. L. Jirtle, "The measured electrical properties of normal and malignant human tissues from 50 to 900 MHz," *Med. Phys.*, Vol. 21, No. 4, 547–550, 1994.
2. Lazebnik, M., D. Popovic, L. McCartney, C. B. Watkins, M. J. Lindstrom, J. Harter, S. Sewall, T. Ogilvie, A. Magliocco, T. M. Breslin, W. Temple, D. Mew, J. H. Booske, M. Okoniewski, and

S. C. Hagness, "A large-scale study of the ultrawideband microwave dielectric properties of normal, benign and malignant breast tissues obtained from cancer surgeries," *Phys. Med. Biol.*, Vol. 52, No. 20, 6093–6115, 2007.

3. Li, Z., W. Wang, Z. Cai, S. Han, S. Lin, L. He, M. Chen, D. Pan, G. Deng, S. Duan, and S. X. Xin, "Variation in the dielectric properties of freshly excised colorectal cancerous tissues at different tumor stages," *Bioelectromagnetics*, Vol. 38, No. 7, 522–532, 2017.
4. Zhang, X., J. Liu, and B. He, "Magnetic-resonance-based electrical properties tomography: A review," *IEEE Rev. Biomed. Eng.*, Vol. 7, 87–96, 2014.
5. Katscher, U. and C. A. T. van den Berg, "Electric properties tomography: Biochemical, physical and technical background, evaluation and clinical applications," *NMR Biomed.*, Vol. 30, No. 8, 1–15, 2017.
6. Liu, J., Y. Wang, U. Katscher, and B. He, "Electrical properties tomography based on B1 maps in MRI: Principles, applications, and challenges," *IEEE Trans. Biomed. Eng.*, Vol. 64, No. 11, 2515–2530, 2017.
7. Schenck, J. F., "The role of magnetic susceptibility in magnetic resonance imaging: MRI magnetic compatibility of the first and second kinds," *Med. Phys.*, Vol. 23, No. 6, 815–850, 1996.
8. Haacke, E. M., L. S. Petropoulos, E. W. Nilges, and D. H. Wu, "Extraction of conductivity and permittivity using magnetic resonance imaging," *Phys. Med. Biol.*, Vol. 36, No. 6, 723–734, 1991.
9. Wen, H., "Noninvasive quantitative mapping of conductivity and dielectric distributions using RF wave propagation effects in high-field MRI," *Proc. SPIE Med. Imag.*, Vol. 5030, 471–477, San Diego, CA, USA, 2003.
10. Seo, J. K., M.-O. Kim, J. Lee, N. Choi, E. J. Woo, H. J. Kim, O. I. Kwon, and D.-H. Kim, "Error analysis of nonconstant admittivity for MR-based electric property imaging," *IEEE Trans. Med. Imag.*, Vol. 31, No. 2, 430–437, 2012.
11. Hafalir, F. S., O. F. Oran, N. Gurler, and Y. Z. Ider, "Convection-reaction equation based magnetic resonance electrical properties tomography (cr-MREPT)," *IEEE Trans. Med. Imag.*, Vol. 33, No. 3, 777–793, 2014.
12. Balidemaj, E., C. A. van den Berg, J. Trinks, A. L. van Lier, A. J. Nederveen, L. J. A. Stalpers, H. Crezee, and R. F. Remis, "CSI-EPT: A contrast source inversion approach for improved MRI-based electric properties tomography," *IEEE Trans. Med. Imag.*, Vol. 34, No. 9, 1788–1796, 2015.
13. Arduino, A., L. Zilberti, M. Chiampi, and O. Bottauscio, "CSI-EPT in presence of RF-shield for MR-coils," *IEEE Trans. Med. Imag.*, Vol. 36, No. 7, 1396–1404, 2017.
14. Hampe, N., M. Herrmann, T. Amthor, C. Findeklee, M. Doneva, and U. Katscher, "Dictionary-based electric properties tomography," *Magn. Reson. Med.*, Vol. 81, No. 1, 342–349, 2018.
15. Nara, T., T. Furuichi, and M. Fushimi, "An explicit reconstruction method for magnetic resonance electrical property tomography base on the generalized Cauchy formula," *Inverse Problems*, Vol. 33, No. 10, 105005, 2017.
16. Fushimi, M. and T. Nara, "A boundary-value-free reconstruction method for magnetic resonance electrical properties tomography based on the Neumann-type integral formula over a circular region," *SICE JCMSI*, Vol. 10, No. 6, 571–578, 2017.
17. Vekua, I., *Generalized Analytic Functions*, Pergamon Press, 1962.
18. Katscher, U., T. Voigt, C. Findeklee, P. Vernickel, K. Nehrke, and O. Dössel, "Determination of electric conductivity and local SAR via B1 mapping," *IEEE Trans. Med. Imag.*, Vol. 28, No. 9, 1365–1374, 2009.
19. Gurler, N. and Y. Z. Ider, "Numerical methods and software tools for simulation, design, and resonant mode analysis of radio frequency birdcage coils used in MRI," *Concepts Magn. Reson. Part B*, Vol. 45B, No. 1, 13–32, 2015.
20. Shepp, L. A. and B. F. Logan, "The Fourier reconstruction of a head selection," *IEEE Trans. Nucl. Sci.*, Vol. 21, No. 3, 21–43, 1974.
21. Insko, E. K. and L. Bolinger, "Mapping of the radiofrequency field," *J. Magn. Reson.*, Vol. 103, No. 1, 82–85, 1993.